Iron-Ions and Iron-Hydroxides Adsorption to Charge-Neutral Phosphatidylcholine Templates

Wenjie Wang,[*,†] Honghu Zhang,[‡] Shuren Feng,[¶] Josue San Emeterio,[†] Surya Mallapragada,[§] and David Vaknin[*,‖]

†*Division of Materials Sciences and Engineering, Ames Laboratory, USDOE, Ames, Iowa 50011, United States*

‡*Ames Laboratory, and Department of Materials Science and Engineering, Iowa State University, Ames,Iowa 50011, United States*

¶*Ames Laboratory, and Roy J. Carver Department of Biochemistry, Biophysics and Molecular Biology, Iowa State University, Ames, Iowa 50011, United States*

§*Ames Laboratory, and Department of Chemical and Biological Engineering, Iowa State University, Ames, Iowa 50011, United States*

‖*Ames Laboratory, and Department of Physics and Astronomy, Iowa State University, Ames, Iowa 50011, United States*

E-mail: wwang@ameslab.gov; vaknin@ameslab.gov

Abstract

Surface sensitive X-ray scattering and spectroscopy techniques reveal significant adsorption of iron ions and iron-hydroxide (Fe(III)) complexes to a charge neutral zwitterionic template of phosphatidylcholine (PC). The PC template is formed by a Langmuir monolayer of di-palmitoyl-PC (DPPC) that is spread on the surface of 2 to 40 μM $FeCl_3$ solutions at physiological levels of KCl (100 mM). At 40 μM of Fe(III) as many as $\sim$ 3 iron atoms are associated with each PC group. Grazing incidence x-ray diffraction measurements indicate a significant disruption in the inplane ordering of DPPC molecules upon iron adsorption. The binding of iron-hydroxide complexes to a neutral PC surface is yet another example of non-electrostatic, presumably covalent bonding to a charge-neutral organic template. The strong binding and the disruption of in-plane lipid structure has biological implications on the integrity of PC-derived lipid membranes including those based on sphingomyelin.

Keywords: Ion-specific binding, Charge neutral membrane, Phosphatidylcholine-iron interactions, Membrane iron-disruption

Graphical TOC Entry

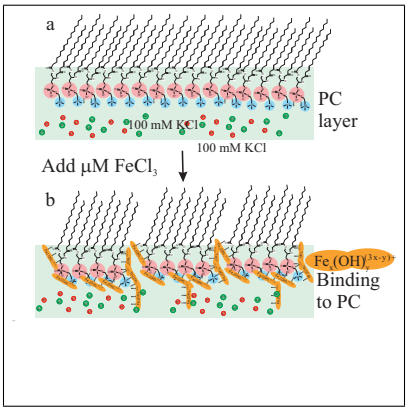

Introduction

Recently, there has been a growing interest in elucidating the adsorption of iron ions and its hydrolysis complexes in solutions to bio-mimetic templates.[1–7] Although, driven to better understand the strong specific Fe-binding to a protein that promotes the growth of magnetite nano-crystals in magnetotactic bacteria (Mms6),[8–11] these control studies have brought about some remarkable results. For instance, for a two-dimensional (2D) neutral carboxylic-group-template (formed by a Langmuir monolayer of arachidic-acid at low pH levels; pH $\sim$ 3), it has been found that a few layers of iron complexes are bound to the surface most likely covalently.[1,2] Carboxylic groups, the likely Fe binding sites of the Mms6 protein, attract Fe complexes more strongly than other trivalent (La^{3+}) or divalent (Ca^{2+} or Fe^{2+}) ions.[3] Extending the studies to a template that is formed by a Langmuir monolayer of di-hexadecyl phosphate, also at low pH values, where theoretical calculations based on Poisson-Boltzmann theory and experimental results using La^{3+} ions in solution clearly indicate that the template is electrostatically neutral, also show strong binding of iron complexes at the interface.[2] Here, we explore the binding of iron ions (Fe(III)) to the biologically relevant phosphatidylcholine (PC) template using physiological levels of KCl (i.e., 100 mM at low pH $\sim$ 3). The effect of divalent cations on PC-based membranes and templates have been studied and have shown to induce conformational and hydration changes in the PC region due to presumable interaction between the phosphate group and the cation,[12,13] that for multi-bilayer lipids, the cations tend to increase the transition temperature from gel-to-liquid-crystalline (LR). To determine the structure and composition of a di-palmyitoyl-phosphatidylcholine (DPPC) that is spread as a Langmuir monolayer (ML) at the vapor/solution (100 mM KCl and sub-mM $FeCl_3$) interface at low pH values at which the phosphate group is protonated, we employ surface sensitive X-ray diffraction and spectroscopic techniques[14–19] . Similar studies have been reported on various divalent ions with PC-based lipid monolayers albeit at relatively high salt concentrations ($\sim$ 0.1 M; much higher than those in living cells),[20,21] showing changes in $\pi - A$ isotherms but insignificant structural effects in the X-ray reflectivity or

grazing incidence diffraction (GIXD). This is not surprising considering a recent molecular-dynamic simulations that show strong competition between cation binding to PC and to water molecules.[22] Here, in addition to X-ray reflectivity (XR) and GIXD, we use X-ray near-total-reflection fluorescence (XNTRF) spectroscopy to specifically and qualitatively monitor interfacial ion accumulation from dilute iron solutions. As we discuss below the results have biological implications as the PC group is shared by other phospholipids including sphingomyelin.

Experimental Methods

Reagents and Materials: 1,2-dipalmitoyl-sn-glycero-3-phosphocholine (DPPC, $C_{40}H_{80}NO_8P$; molecular weight 734.039 g/mol; CAS No.63-89-8) was purchased from Avanti Polar Lipids, Inc. and dissolved in 3:1 chloroform/methanol solution for surface spreading. Ultrapure water (Millipore, Milli-Q, and NANOpure, Barnstead; resistivity 18.1 MΩ cm) was used in all suphase solution preparations. Iron chloride ($FeCl_3{\cdot}6H_2O$, CAS No.10025-77-1, purchased from Fisher Scientific) subphase solutions were prepared from the same parent solution and diluted to the desired concentrations. The iron solutions were maintained at pH 3 by addition of hydrochloric acid (HCl). Additional 100 mM potassium chloride (KCl, CAS No.7447-40-7, purchased from Fisher Scientific) were present in all iron solutions to mimic the physiological conditions. These conditions have been used to complement and compare studies of Fe(III) binding to Mms6 under conditions that have been used for iron oxide crystal formation promoted by this protein in vitro.[11]

X-ray Scattering Setup Synchrotron-based X-ray measurements were performed on the liquid surface spectrometer (LSS) at the 9-ID-C beamline at the Advanced Photon Source (APS), Argonne National Laboratory using incident X-ray energy $E = 13.474$ keV (corresponding wavelength $\lambda = 0.9201$ Å). The aqueous $FeCl_3$ subphase solutions were contained in a Langmuir trough mounted on the LSS. The DPPC in chloroform/methanol (3:1) stock

solution was spread on the aqueous surface in a sealed Langmuir trough that was purged with water-saturated helium to minimize potential radiation damage to the sample surface and reduce background scattering from air. The spread monolayer (ML) is compressed with a motorized Teflon barrier and surface pressure is measured with a filter-paper Wilhelmy plate to obtain surface-pressure versus molecular area ($\pi - A$) isotherms. During the X-ray measurements the monolayer is maintained at a constant pressure (within predetermined experimental tolerance $\pm$ 3 mN/m; the surface pressure of the monolayers during measurements has been stable to better than $\pm$1 mN/m). A highly collimated and monochromatic X-ray beam of wave vector $\mathbf{k}_\mathrm{i}$ is steered onto the surface at an incident angle α_i. More details on the experimental methods and techniques can be found in the Supporting Information.

Results and Discussion

Surface Pressure-Area Isotherms

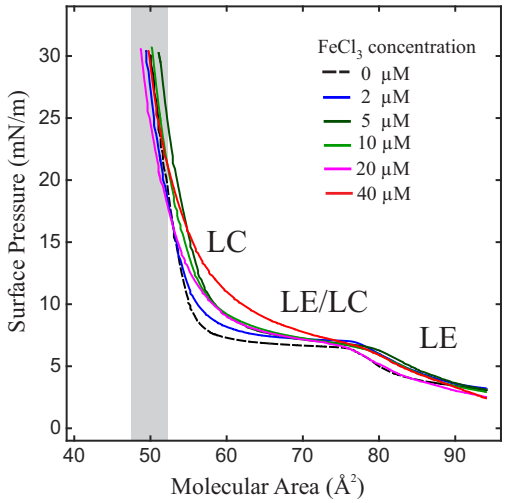

Figure 1: Surface pressure *versus* molecular area isotherms of DPPC on aqueous subphase solutions of $FeCl_3$ at concentrations from 0 up to 40 μM as indicated. Shaded area indicates the range of the surface-pressure and molecular area of DPPC in the course of the X-ray measurements. All solutions also included 100 mM KCl at pH 3.

Surface pressure (Π) *versus* molecular area (A_mol) isotherms for DPPC on 100 mM KCl at various concentrations of $FeCl_3$ (in the micromolar range) solutions are shown in Fig. 1. The

isotherm of DPPC, is typical of other phospholipids on pure aqueous solutions exhibiting liquid-expanded (LE), liquid-condensed (LC) , and the LE/LC (coexisting phases plateau on the isotherms) phases.[23,24] The isotherm in our study does not seem to be affected by the presence of KCl as shown in Fig. 1, however, micromolar level concentrations of iron have a modest effect on the coexistence LE/LC phase such that higher concentrations of iron gradually narrow this phase (i.e., the plateau region in the isotherms). This behavior indicates the formation of LC clusters at large molecular areas due to the tethering caused by iron-complexes binding. We note that the molecular area of DPPC reaches ~ 50 Å^2 at $\Pi \sim 30 \pm 3$ mN/m, at the point on the isotherms where the X-ray measurements have been conducted.

X-ray Reflectivity

Table 1: DPPC monolayer structural parameters extracted from the refinement of R/R_F data. The monolayer is modeled as a three-slab stratum. The subscript 1 to 3 represent the layer in contact with the subphase[a], the layer just below the hydrocarbon tails and the hydrocarbon chains in contact with vapor phase.

[$FeCl_3$] (μM)	0	2	10	40
d_1 (Å)	15^{+2}_{-2}	15^{+1}_{-1}	$9.6^{+1.3}_{-0.5}$	$9.2^{+0.2}_{-0.2}$
ρ_1 e/Å^3	$0.348^{+0.001}_{-0.001}$	$0.372^{+0.002}_{-0.005}$	$0.410^{+0.003}_{-0.002}$	$0.395^{+0.001}_{-0.001}$
d_2 (Å)	$9.2^{+0.8}_{-1.1}$	$8.9^{+1.6}_{-1.4}$	$13.9^{+0.8}_{-2.3}$	$18.8^{+0.2}_{-0.1}$
ρ_2 (e/Å^3)	$0.50^{+0.04}_{-0.02}$	$0.55^{+0.04}_{-0.05}$	$0.53^{+0.04}_{-0.01}$	$0.55^{+0.01}_{-0.01}$
d_3 (Å)	$15.2^{+0.4}_{-0.4}$	$16.3^{+0.5}_{-0.5}$	$17.3^{+0.7}_{-0.2}$	$19.0^{+0.2}_{-0.1}$
ρ_3 e/Å^3	$0.28^{+0.03}_{-0.02}$	$0.26^{+0.03}_{-0.02}$	$0.252^{+0.006}_{-0.002}$	$0.39^{+0.01}_{-0.03}$
σ (Å)	$3.3^{+0.2}_{-0.2}$	$3.8^{+0.2}_{-0.3}$	$3.6^{+0.3}_{-0.1}$	$4.0^{+0.1}_{-0.1}$

[a] The addition of this slab that is in contact with the subphase, compared to the two-slab model that depicts the DPPC monolayer on pure water,[25] is found to improve the reflectivity fitting substantially. The slightly higher ED in the slab adjacent to subphase may indicate minute inclusion of excess K^+ and/or Cl^-, reorientation and reorganization of adjacent water molecules, or rearrangement of the head group, compared to the DPPC on pure water subphase.[25]

Figure 2 shows the measured normalized reflectivity R/R_F for monolayers on the $FeCl_3$ subphase at concentrations from 0 to 40 μM as indicated. The XR from the monolayer on the 100 mM KCl solution is very similar to that measured on water[25] (i.e., the Q_z

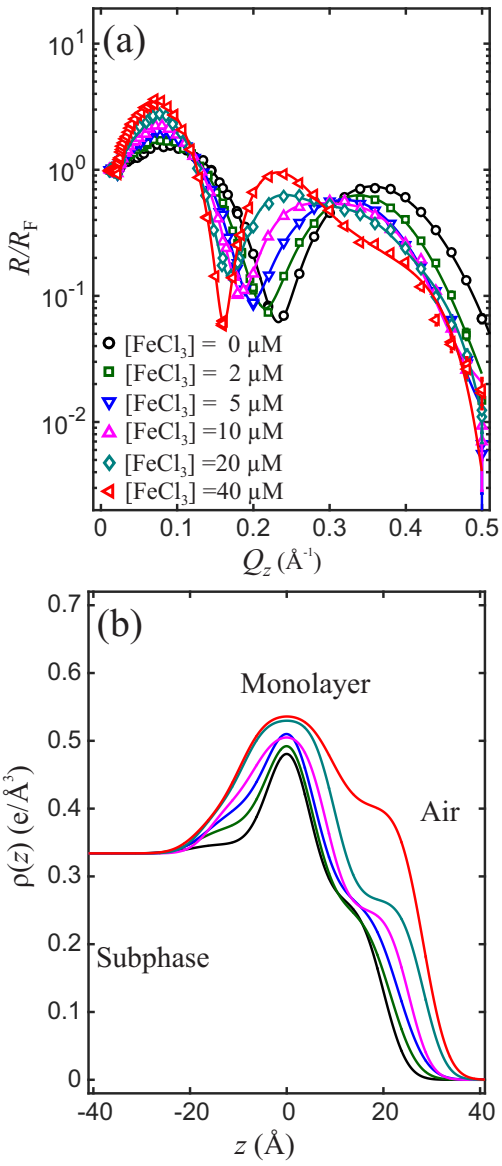

Figure 2: (a) Normalized reflectivity data from DPPC monolayers on $FeCl_3$ subphase of concentration $0-40$ μM as indicated. The solid lines through data points are calculated R/R_F using the best-fit parameters. (b) The electron density (ED) profiles, $\rho(z)$, corresponds to the best-fit R/R_F in (a). The ED profiles are shifted horizontally to make the ED maxima coincide at $z = 0$ for display purposes.

where the first reflectivity maximum and minimum occur barely changes in the presence and absence of KCl). Qualitatively, two systematic trends can be identified upon increasing iron concentrations; one is a shift of the first minimum in the R/R_{F} towards lower Q_z values, and the second is a gradual increase in the first maximum near the critical angle. These indicate a gradual increase in film thickness and a higher electron density in the head group region upon increasing subphase iron concentrations, respectively, evidence for interfacial accumulation of iron ions and/or their complexes at the interface.[14] DPPC monolayer structure at the air-water interface has been characterized with a combined X-ray and neutron reflectivity methods,[25] in which the two-slab model has been used to extract the head group size, chain-length and -tilt angle. In view of the more complex head group and its interaction with iron influenced by pH and other ions, in our analysis we parse the DPPC-iron film into three slabs to better refine the reflectivity data. The solid lines in Fig. 2(a) are the best-fit calculated reflectivities obtained from the corresponding electron density (ED) profiles across the interface shown in Fig. 2(b) and constructed with the parameters in Table 1 for selected iron bulk concentrations. Three regions, i.e., the subphase, monolayer (consisting of head groups and tail groups) and air, can be readily recognized on the ED profiles. All density profiles show an increase in film thickness with respect to the monolayer in the absence of iron, but more importantly they also show a significant increase in electron density at the head group region. Below 20 μM, the increase in the ED is significant in the strata that represent the PC headgroup and its immediate neighboring region in the subphase. This we interpret as evidence for direct iron binding to the headgroup region and to protruding iron complexes that extend from some headgroups, respectively. However, a dramatic change in the ED profile is observed for DPPC ML on 40 μM iron solution with a much higher electron density on both sides of the headgroup. This suggests significant enrichment at the surface with bound iron-complexes that likely occupy the space originally for the hydrocarbon region of the DPPC and affect the in-plane packing of the DPPC film. The XR, although demonstrating iron binding that increases the ED over that of water and the headgroup,

does not specifically provide information on the nature of the elemental species that enrich the interface; the XNTRF discussed below provides such information.

X-ray Fluorescence

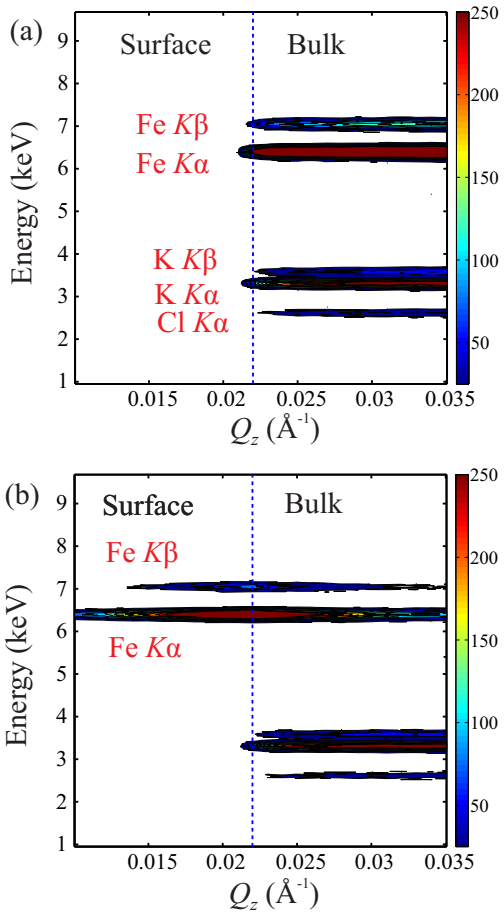

Figure 3: Two dimensional color map representing fluorescence intensity data collected for (a) a $FeCl_3$ solution (5 mM) of bare surface and (b) a dilute $FeCl_3$ solution (40 μM) in the presence of DPPC monolayer. The fluorescence intensities (in arbitrary units) are presented as a function of the energy of fluorescence X-rays collected by EDD at a series of Q_z that represent equivalent grazing incidence angles. The vertical dashed lines represent the Q_z corresponding to the critical angle α_c.

Figure 3 (a) and (b) show the fluorescence spectra collected at a series of α_i (or Q_z; see definitions in the SI) for $FeCl_3$ solutions in the absence and presence of the DPPC monolayer combined into a color map. For a bare surface (no DPPC ML; with 5 mM $FeCl_3$ and 100 mM KCl in the solution; Fig. 3(a)) we observe the $K\alpha$ and $K\beta$ emission lines from K, Cl and Fe as indicated. Note that the fluorescence signals below the critical angle (indicated by dashed line) are not visible in the spectra, because the minute amount of fluorescing

elements at the evanescent penetration depth ($\approx$ 85 Å) is beyond the detection limit of our detector. Above the critical angle, the X-rays penetrate into the bulk water with micron length scale penetration depth and the characteristic emission lines, i.e., $K\alpha$ and $K\beta$ of iron ($\sim$ 6.40 and 7.06 keV), potassium ($\sim$ 3.31 and 3.59 keV), and chlorine ($\sim$ 2.62 and 2.82 keV; unresolved), are evident in the spectra. The fluorescence intensity from the bulk (Fig. 3 (a) for 5 mM $FeCl_3$) to a good approximation scales with concentration. Therefore, for bare surface solutions of micromolar Fe(III) (without the monolayer) the signal is at background level from the surface or bulk (i.e., below or above the critical angle; data not shown). However, in the presence of a DPPC monolayer, under otherwise identical conditions, there are strong signals from iron peaked at the critical angle clearly indicating that they emanate from irons at the interface. The signals over the whole Q_z range and the peak intensity at the critical angle are evidence for surface enrichment of iron in the proximity of the head group (more quantitative details below). Iron emission lines integrated over Q_z range from 0.017 to 0.019 $Å^{-1}$ (corresponding $\alpha_i = 0.069 - 0.080°$) for various Fe concentrations as indicated with a DPPC ML and from 5 mM without the ML are shown in Fig. 4. Notice that the signal below the critical angle is highly sensitive to ions at the interface, such that even 5 mM $FeCl_3$ in solution show almost no signal (black symbols in Fig. 4) compared to the 2μM with DPPC at the surface. By contrast, there is no detectable signal from K^+ or Cl^- below the critical angle, even though these ions are at moderate concentrations in the solutions, indicating that the amount of surface-enriched K^+ or Cl^-, if any, is below the instrumental detection limit.[29] The observation of iron surface enrichment in the presence of a charge neutral interface suggests that iron (and iron-hydroxide complexes) binding to PC is not electrostatic in nature as has also been reported for similar neutral membranes.[1,2]

The surface excess of iron atoms, denoted as Γ, can be quantitatively determined through the analysis of the angular dependence (i.e., Q_z) of the fluorescence intensity.[2,26] As first approximation, we consider that the fluorescence signal emanates equivalently from a plane that is buried under the monolayer-air interface, i.e., the distribution of surface bound, ex-

Table 2: Surface excess (Γ) and depth of iron atoms ($z_{\rm ion}$) extracted from the fluorescence data collected below the critical angle.[a,b]

[Fe^{3+}] (μM)	$\Gamma(\times 10^{-2}$ Å$^{-2})$	$N_{\rm ions}$	$z_{\rm ion}$ (Å)
2	0.8 (±5%)	0.4 (±0.1)	30 (±15%)
5	1.5 (±3%)	0.8 (±0.1)	29 (±10%)
10	2.1 (±4%)	1.0 (±0.15)	31 (±11%)
20	3.6 (±3%)	1.8 (±0.2)	36 (±9%)
40	5.6 (±2%)	2.9 (±0.2)	37 (±6%)

[a] The fluorescence intensities obtained below the critical angle for total reflection (over Q_z range $0.010 - 0.021$Å^{-1}) are assumed to emanate from a thin layer of iron located at a depth of $z_{\rm ion}$ from the monolayer-air interface (i.e., depth profile of iron surface enrichment is reduced to a Dirac-$\delta(z)$ function). Its angular-dependence is expressed as $C|T(\alpha_{\rm i})|^2\Gamma\exp[-z_{\rm ion}/D(\alpha_{\rm i})]$, where $T(\alpha_{\rm i})$ is Fresnel amplitude transmission function,[16] $D(\alpha_{\rm i})$ the X-ray penetration depth along the surface normal.[16,17] The intensity scaling factor, C, can be obtained from the angular-dependent fluorescence intensity from a bulk iron solution (bare surface) of know concentration n_b, expressed as $C|T(\alpha_{\rm i})|^2 n_b D(\alpha_{\rm i})$. More examples can be found elsewhere.[1,2,26,28]

[b] $N_{\rm ions}$ is the number of bound ions per DPPC molecule extracted from Γ and an average molecular area of 50 Å^2.

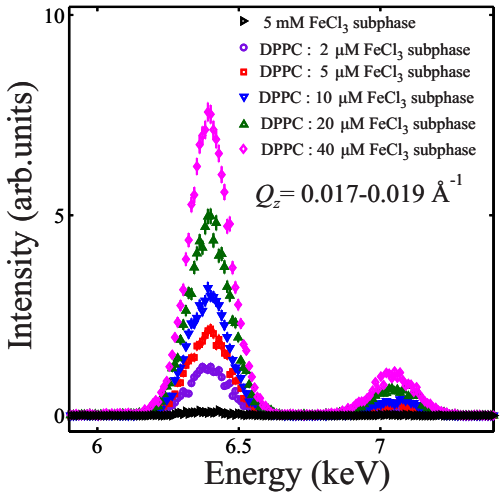

Figure 4: Fluorescence spectra (i.e., $K\alpha$ and $K\beta$ emission lines of interfacial Fe) collected at incident angles below the critical-angle for total reflection. Each data point is the intensity integrated over $Q_z = 0.017 - 0.019$ Å^{-1} (corresponding $\alpha_{\rm i} = 0.069 - 0.080^\circ$). Intensities of emission lines are normalized to the incident beam intensity.

cess iron atoms are modeled as residing uniformly on a plane (with planar density Γ) that is a distance z_{ion} below the air/monolayer interface,[2] which is consistent with the XRR results that the ED enhancement is mainly restricted to the headgroup region. The average surface excess density of the ions (Γ) and their average position with respect to the hydrocarbon-chains/vapor-interface (z_{ion}) are summarized in Table 2. Also, provided in Table 2 is the average number of iron ions per PC group (N_{ions}) evaluated from Γ and assuming the molecular area for all concentrations is $\sim$ 50 Å^2 (consistent with the isotherms and the GIXD below). At the higher concentrations, the observation of the large number of iron ions ($\sim$ 3) per PC group suggests that the complexed clusters are bound to the PC group. Such phenomena of iron complexes binding under similar conditions to neutral caboxylic or phosphate templates have been explained as resulting from effective covalent bonding of iron precipitates such as $Fe(OH)_3(s)$ and $Fe_x(OH)_y^{(3x-y)+}$ clusters. Figure 5 shows the various iron species in aqueous solutions of $FeCl_3$ in the concentration range used in this study and at pH 3, indicating the prevalence of positively charged species and minute amounts of $Fe(OH)_3$. More details on the character and calculation of the species in the solution[34–37] is provided in the SI. We note that the surface-bound iron depth profiles cannot be uniquely determined with the current data sets.

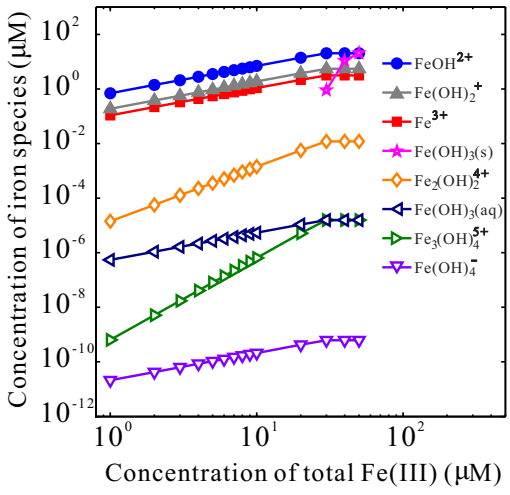

Figure 5: Calculated concentrations of various iron species formed in the aqueous solution of $FeCl_3$ maintained at pH 3.0.

Grazing Incidence Diffraction

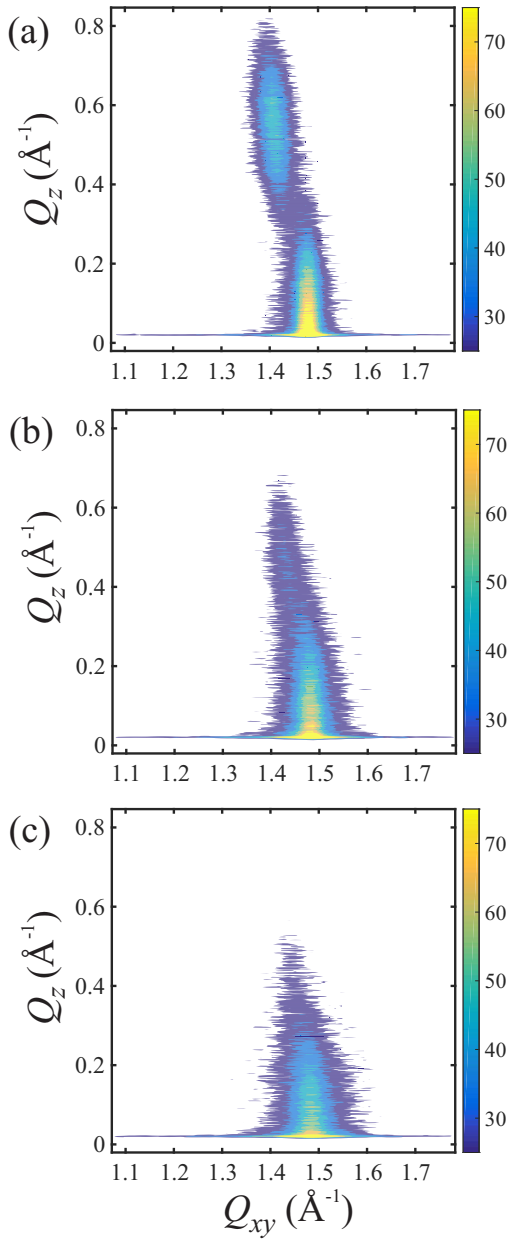

Figure 6: Two-dimensional intensity contour plot for grazing incidence diffraction from DPPC monolayer on $FeCl_3$ solutions at concentrations of (a) 2 μM (b) 10 μM and (c) 40 μM.

Figure 6 shows the GIXD contour plots for DPPC monolayers on subphase of iron solutions as indicated. For the DPPC monolayer on iron solutions as dilute as 2 μM, the observation of two Bragg rods, one emanating from $Q_z \approx 0$ and the second centered at $Q_z \approx 0.55$ Å^{-1}, is consistent with other reports on DPPC MLs on water or on mono- and

di-valent ions, at similar surface pressures as shown in Fig. 6(a).[27,30–33] The one located at $Q_{xy} = Q_{xy}^{\rm hk} \approx 1.41$ Å^{-1} and $Q_z = Q_z^{\rm hk} \approx 0.55$ Å^{-1} is indexed as (hk)=(11), and the other located at $Q_{xy} = Q_{xy}^{\rm hk} \approx 1.48$ Å^{-1} and $Q_z = Q_z^{\rm hk} \approx 0$ indexed as (hk)=(02), according to the Miller indices for the 2D centered rectangular lattice type. The d-spacings, i.e., $d_{11} = 2\pi/Q_{xy}^{11} \approx 4.46$ Å and $d_{02} = 2\pi/Q_{xy}^{02} \approx 4.25$ Å, corresponding to a rectangular unit cell of the chains with the edge length $a \approx 5.24$ Å and $b \approx 8.49$ Å. The (11) Bragg-peak at a finite Q_z-axis indicates tilted hydrocarbon chains to nearest-neighbor (NN) by an angle t, given by $t = \tan^{-1}(Q_z^{11}/\sqrt{(Q_{xy}^{11})^2 - (Q_{xy}^{02})^2/4})$.[14,16,17,19] The area of the tilted unit cell, $A_{\rm GIXD} = ab \approx 45$ Å^2, roughly corresponds to the average molecular area $A_{\rm mol}$.

Table 3: In-plane structural parameter of DPPC in the presence of iron in the subphase (using rectangular symmetry notation).

[$FeCl_3$] (μM)	d-spacing (Å) [a]	Tilt angle t [b]	$A_{\rm GIXD}$ (Å^2)
2	$d_{11} = 4.46$ $d_{02} = 4.25$	24.6°	44.5
5	$d_{11} = 4.42$ $d_{02} = 4.24$	22.4°	43.9
10	$d_{11} = 4.38$ $d_{02} = 4.23$	20.1°	43.3
20	$d_{11} = 4.38$ $d_{02} = 4.24$	20.1°	43.4
40	$d_{11} = 4.38$ $d_{02} = 4.23$	22.2°	43.3

[a] The Miller indices for d-spacing are based on rectangular unit cell.

[b] The nearest-neighbor (NN) tilt is used to determine the tilt angle. The relative uncertainty is ±15%.

Upon increasing iron bulk concentration, the (11) Bragg peak becomes weaker and less distinguishable from the (02) peak, as shown in Fig. 6(b) and (c). We analyze the GIXD intensity profile at any given Q_z as a sum of the two Bragg peak profiles, each of which is modeled as a Lorentzian function. The extracted in-plane structural parameters are listed in Table 3. In the absence of (11) Bragg peak, the (02) Bragg peak (indexed using the centered rectangular lattice type) can be interpreted as (10) rod of a hexagonal structure. In general, it is known that the molecular area extracted from the GIXD underestimates the average

area obtained in the isotherms, since the GIXD ignores domain boundaries and voids. More importantly, consistently the line-width of the (02) gets broadened as the iron concentration increases indicating deterioration of in-plane ordering (including both collective tilt and un-tilt phases) as iron binds to the film. This is consistent with the ED obtained from the XR that shows some penetration of iron-complexes to the space originally occupied by hydrocarbon regions. Figure 7 depicts the DPPC monolayer at the liquid/vapor interface on 100 mM KCl solution at the crystalline phase. The monolayer is highly uniform with hydrocarbon chains that are tilted to an almost 30° angle with respect to the surface normal. The addition of minute amounts of $FeCl_3$ leads to the binding of iron compmlexes to the PC and possibly to the glycerol groups lowering the chain tilt angle and at the same time breaking the film into smaller domains and increasing the inhomogeneity of the membrane .

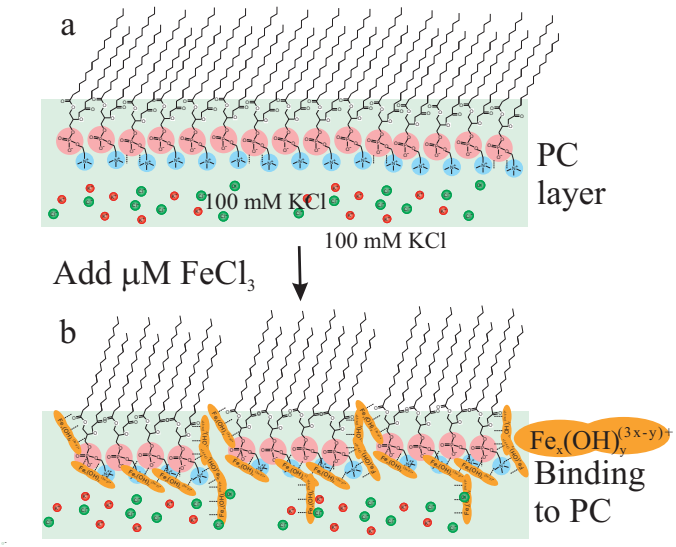

Figure 7: (a) Schematic illustration of a DPPC monolayer at the liquid/vapor interface on 100 mM KCl solution at the crystalline phase. The monolayer is highly uniform with hydrocarbon chains that are tilted to an almost 30° angle with respect to the surface normal. (b) With the addition of minute amounts of $FeCl_3$ iron compmlexes bind to the PC and possibly to the glycerol groups lowering the chain tilt angle and at the same time disturbing the uniformity of the membrane.

Conclusion

Using synchrotron X-ray reflectivity, grazing incidence diffraction and fluorescence techniques we determine quantitatively the mutual effect between dilute iron ions and its complexes in solutions and a neutrally charged phosphatidylcholine template formed by a DPPC monolayer at the vapor/liquid interface. Our X-ray fluorescence results show that significant amount of iron ions and/or iron-hydroxide complexes bind and form a contiguous layer at the headgroups of the neutral DPPC monolayer. The accumulation and binding of iron at the interface increases with the concentration, so that at 40 μM there are close to three iron atoms per DPPC molecule. We emphasize that in subsequent control experiments with similar PC templates we find that the presence of salt (i.e., 100 mM KCl, NaCl or other salts of similar ionic strength) is necessary for the iron binding to PC (data not shown). Our GIXD shows that the hydrocarbon chains of the DPPC are crystalline at low concentration levels, but for higher concentrations the in-plane correlations become shorter (domains become smaller) due to the formation of disordered iron-hydroxides network. We surmise that iron binding to PC affects the fluidity and the uniformity of the PC membrane by forming imobolized smaller crystalline domains that are surrounded by iron-complexes. Considering that the cytoplasmic side of mammalian cell membranes are also rich in potassium ions, and that iron is an essential metal element that is involved in multiple cellular activities, these results have significant implications on the effect that iron-complexes may have on uncharged regions in cell membranes. In addition to blocking neutrally charged regions, Fe(III) also tends to deteriorate the intactness of the membrane. This is an important result considering the fact that PC group is also present in other phospholipids in particular in sphingomyelin, a major constituent of the myelin sheath.

Acknowledgement

We thank Dr. Ivan Kuzmenko for technical help at the 9ID-B,C beamline of the Advanced Photon Source, Argonne National Laboratory. H. Z. thanks Prof. Mufit Akinc (Ames Laboratory and Iowa State University) for discussions on the hydrolysis of iron. J. S. thanks the support from the Science Undergraduate Laboratory Internship (SULI) program of U.S. Department of Energy. Research was supported by the U.S. Department of Energy, Office of Basic Energy Sciences, Division of Materials Sciences and Engineering. Ames Laboratory is operated for the U.S. Department of Energy by Iowa State University under Contract No. DE-AC02-07CH11358. Use of the Advanced Photon Source, an Office of Science User Facility operated for the U.S. Department of Energy (DOE) Office of Science by Argonne National Laboratory, was supported by the U.S. DOE under Contract No. DE-AC02-06CH11357.

Supporting Information Available

Details of experimental methods on surface sensitive X-ray scattering and spectroscopy techniques (XR, XNTRF and GIXD) and on the hydrolysis of Fe(III) are provided in the Supporting Information.

This material is available free of charge via the Internet at `http://pubs.acs.org/`.

References

(1) Wang, W.; Park, R. Y.; Travesset, A.; Vaknin, D. Ion-specific induced charges at aqueous soft interfaces. *Phys. Rev. Lett.* **2011**, *056102*.

(2) Wang, W.; Park, R. Y.; Meyer, D. H.; Travesset, A.; Vaknin, D. Ionic specificity in pH regulated charged interfaces: Fe^{3+} versus La^{3+}. *Langmuir* **2011**, *27*, 11917-11924.

(3) Wang, W.; Bu, W.; Wang, L.; Palo, P. E.; Mallapragada, S.; Nilsen-Hamilton, M.; Vaknin, D.Interfacial properties and iron binding to bacterial proteins that promote the growth of magnetite nanocrystals: X-ray reflectivity and surface spectroscopy studies *Langmuir* bf 2012, *28*, 4274 - 4282.

(4) Wang, W.; Pleasants, J.; Bu, W.; Park, R. Y.; Kuzmenko, I.; Vaknin, D. Amoprhous iron-(hydr) oxide networks at liquid/vapor interfaces: In situ X-ray scattering and spectroscopy studies. *J. Colloid Interface Sci.* **2012**, *384*, 45-54.

(5) Wieland, D. C. F.; Degen, P.; Paulus, M.; Schroer, M. A.; Bieder, S.; Sahle, C. J.; Moller, J.; Leick, S.; Chen, Z.; Struth, B.; Rehage, H.; Tolan, M. Formation of iron containing aggregates at the liquid-air interface. *Coll. Surf. B-Biointerfaces*, **2013**, *109*, 74-81.

(6) Stefaniu, C.; Brezesinski, G.; Moehwald, H., Langmuir monolayers as models to study processes at membrane surfaces. *Adv. Coll. Inter. Sci.* **2014**, *208*, 197-213.

(7) Stefaniu, C.; Brezesinski, G. X-ray investigation of monolayers formed at the soft air/water interface. *Curr. Opin. Coll. Inter. Sci.* **2014**, *19*, 216-227.

(8) Arakaki, A.; Webb, J.; Matsunaga, T. A Novel Protein Tightly Bound to Bacterial Magnetic Particles in Magnetospirillum magneticum Strain AMB-1. *J. Biol. Chem.* **2003**, *278*, 8745.

(9) Amemiya, Y.; Arakaki, A.; Staniland, S. S.; Tanaka, T.; Matsunaga, T. Controlled formation of magnetite crystal by partial oxidation of ferrous hydroxide in the presence of recombinant magnetotactic bacterial protein Mms6. *Biomaterials* **2007**, *28*, 5381.

(10) Arakaki, A.; Masuda, F.; Amemiya, Y.; Tanaka, T.; Matsunaga, T. Control of the morphology and size of magnetite particles with peptides mimicking the Mms6 protein from magnetotactic bacteria. *J. Colloid Interface Sci.* **2010**, *343*, 65.

(11) Wang, L.; Prozorov, T.; Palo, P. E.; Liu, X.; Vaknin, D.; Prozorov, R.; Mallapragada, S.; Nilsen-Hamilton, M. Self-assembly and biphasic iron-binding characteristics of Mms6, a bacterial protein that promotes the formation of superparamagnetic magnetite nanoparticles of uniform size and shape. *Biomacromolecules* **2012**, *13*, 98.

(12) Herbette, L.; Napolitano, C. A.; McDaniel, R. V. Direct determination of the calcium profile structure for dipalmitoyllecithin multilayers using neutron diffraction. *Biophys. J.* **1984**, *46* 677-685.

(13) Binder, H.; Zschörnig, O. The effect of metal cations on the phase behavior and hydration characteristics of phospholipid membranes. *Chem. Phys. Lipids* **2002**, *115*, 39-61.

(14) Kjaer, K. Some simple ideas on X-ray reflection and grazing-incidence diffraction from thin surfactant films. *Physica B* **1994**, *198*, 100-109.

(15) Kaganer, V. M.; Möhwald, H.; Dutta, P. Structure and phase transitions in Langmuir monolayers. *Rev. Mod. Phys.* **1999**, *71*, 779-819.

(16) Als-Nielsen, J.; McMorrow, D. *Elements of Modern X-ray Physics*; John Wiley & Sons: England, 2011.

(17) Vaknin, D. In *Characterization of Materials*; Kaufmann, E. N., Ed.; John Wiley & Sons: New York, 2012; Vol.2, pp 1393-1423.

(18) Pershan, P. S.; Schlossman, M. L. *Liquid Surfaces and Interfaces: Synchrotron X-ray Methods*; Cambridge University Press: 2012.

(19) Stefaniu, C.; Brezesinski, G. Grazing incidence X-ray diffraction studies of condensed double-chain phospholipid monolayers formed at the soft air/water interface. *Adv. Colloid Interface Sci.* **2014**, *207*, 265-279.2011.

(20) Kewalramani, S.; Hlaing, H.; Ocko, B. M.; Kuzmenko, I.; Fukuto, M. Effects of Divalent Cations on Phase Behavior and Structure of a Zwitterionic Phospholipid (DMPC) Monolayer at the Air-Water InterfaceThe *J. Phys. Chem. Lett.* **2010**, *1*, 489?495.

(21) Broniatowski, M.; Flasiński, M.; Dynarowicz-Łatka, P.; Majewski, J. Grazing Incidence Diffraction and X-ray Reflectivity Studies of the Interactions of Inorganic Mercury Salts with Membrane Lipids in Langmuir Monolayers at the Air/Water Interface. *J. Phys. Chem. B* **2010**, *114*, 9474-9484.

(22) Yang, J.; Calero, C.; Bonomi, M.; Martí, J. Specific ion binding at phospholipid membrane surfaces. *J. Chem. Theo. Comp.* **2015**, *11*, 4495-4499.

(23) Gorwyn, D.; Barnes, G. T. Interactions of large ions with phospholipid monolayers. *Langmuir* **1990**, *6*, 222-230.

(24) Klopfer, K. J.; Vanderlick, T. K. Isotherms of dipalmitoylphosphatidylcholine (DPPC) monolayers: Features reserved and features obscured. *J. Colloid Interface Sci.* **1996**, *182*, 220-229.

(25) Vaknin, D.; Kjaer, K.; Als-Nielsen, J.; Lösche, M. Structural properties of phosphatidylcholine in a monolayer at the air/water interface. *Biophys. J.* **1991**, *59*, 1325-1332.

(26) Yun, W.; Bloch, J. M. X-ray near total external fluorescence method: Experiment and analysis. *J. Appl. Phys.* **1990**, *68*, 1421-1428.

(27) Aroti,A.; Leontidis, E.; Maltseva, E.; and, Brezesinski, G. Effects of Hofmeister Anions on DPPC Langmuir Monolayers at the Air?Water Interface. *J. Phys. Chem. B*, **2004**, *108* 15238-15245

(28) Tulli, L. G.; Wang, W.; Rullaud, V.; Lindemann, W. R.; Kuzmenko, I.; Vaknin, D. Binding of calixarene-based Langmuir monolayers to mercury chloride is dependent on the amphiphile structure. *RSC Adv.* **2016**, *6*, 9278-9285.

(29) Graber, Z. T.; Wang, W.; Singh, G.; Kuzmenko, I.; Vaknin, D.; Kooijman, E. E. Competitive cation binding to phosphatidylinositol-4, 5-bisphosphate domains revealed by X-ray fluorescence. *RSC Adv.* **2015**, *5*,106536-106542

(30) Dahmen-Levison, U.; Brezesinski, G.; Möhwald, H. Specific adsorption of PLA_2 at monolayers. *Thin Solid Films* **1998**, *327-329*, 616-620.

(31) Lee. K. Y. C.; Gopal, A.; von Nahmen, A.; Zasadzinski, J. A.; Majewski, J.; Smith, G. S.; Howes, P. B.; Kjaer, K. Influence of palmitic acid and hexadecanol on the phase transition temperature and molecular packing of diphamitoylphosphatidyl-choline monolayers at the air-water interface. *J. Chem. Phys.* **2002**, *116*, 774-783.

(32) Wagner, K.; Brezesinski, G. Modifying dipalmitoylphosphatidylcholine monolayers by n-hexadecanol and dipalmitoylglycerol. *Chem. Phys. Lipids* **2007**, *145*, 119-127.

(33) Miller, C. E.; Busath, D. D.; Strongin, B.; Majewski, J. Integration of ganglioside GT_1b receptor into DPPE and DPPC phospholipid monolayers: An X-ray reflectivity and grazing-incidence diffraction study. *Biophys. J.* **2008**, *95*, 3278-3286.

(34) Martell, A. E.; Smith, R. M. *Critical stability constants*; Plenum Press: New York, 1976; Vol. 4, pp 7.

(35) Stefánsson, A. Iron(III) Hydrolysis and Solubility at 25°C. *Environ. Sci. Technol.* **2007**, *41*, 6117-6123.

(36) Alderighi, L.; Gans, P.; Ienco, A.; Peters, D.; Sabatini, A.; Vacca, A. Hyperquad simulation and speciation (HySS): a utility program for the investigation of equilibria involving soluble and partially soluble species. *Coord. Chem. Rev.* **1999**, *184*, 311-318.

(37) Liu, X.; Millero, F.J. The solubility of iron hydroxide in sodium chloride solutions. *Geochim. Cosmochim. Acta.* **1999**, *63*, 3487-3497.